Velocity map imaging of femtosecond photodynamics in CF3I

ARTICLE *in* CHEMICAL PHYSICS LETTERS · SEPTEMBER 2001

Impact Factor: 1.9 · DOI: 10.1016/S0009-2614(01)00865-X

2 AUTHORS:

W.G. Roeterdink
Jilin University
39 PUBLICATIONS **405** CITATIONS
SEE PROFILE

Maurice H M Janssen
VU University Amsterdam
92 PUBLICATIONS **1,485** CITATIONS
SEE PROFILE

7 September 2001

ELSEVIER

Chemical Physics Letters 345 (2001) 72–80

CHEMICAL PHYSICS LETTERS

www.elsevier.com/locate/cplett

Velocity map imaging of femtosecond photodynamics in CF_3I

W.G. Roeterdink, M.H.M. Janssen *

Laser Center and Department of Chemistry, Vrije Universiteit, de Boelelaan 1083, 1081 HV Amsterdam, Netherlands

Received 5 February 2001; in final form 1 June 2001

Abstract

The femtosecond photodynamics of CF_3I were studied employing the velocity mapping ion imaging technique. The angular and velocity distributions of I^+ fragments were obtained as a function of the time delay between a femtosecond pump pulse at 264 nm and a probe pulse at 396 nm. The images reveal a dependence of the three-dimensional recoil distributions on the pump–probe delay time and the mutual polarization direction of pump and probe pulses. The ion velocity images provide information on the competition of different multi-photon pathways producing the ionic fragments. © 2001 Elsevier Science B.V. All rights reserved.

1. Introduction

Photodissociation experiments provide very detailed information on molecular interactions and bondbreaking dynamics. After the invention of the ion imaging technique in photodynamics [1] the subsequent rapid expansion [2] in the field has demonstrated the power of the imaging technique in studying the angular and kinetic energy distribution of photofragments. In parallel to the imaging developments, femtosecond laser techniques have increasingly been applied over the last decade to study photodynamical processes in real time [3]. In addition to the possibility to study dynamics on the timescale of atomic movement, the use of femtosecond pulses may result in molecular dynamics from other processes than a single photon excitation. The high field strength of amplified femtosecond pulses easily induces multi-photon absorption processes in molecules. These multi-photon pathways can compete favorably and interfere with fast (pre)dissociation dynamics occurring at the one-photon level. For instance, a competing multi-photon pathway was observed in a femtosecond pump–probe experiment on methyl iodide using time-of-flight (TOF) ion detection in a molecular beam [4]. In that experiment a two-photon absorption to an excited Rydberg state, followed by predissociation of the parent Rydberg state, was observed to dominate, whereas the one-photon absorption and subsequent ultrafast dissociation via the well-known A-band of methyl iodide could not be observed.

In order to unravel in more detail the dynamics resulting from these competing pathways we have combined velocity map ion imaging detection [5] with the femtosecond pump–probe technique to study in real-time photon induced dynamics in small molecular systems. The more conventional ion TOF technique, which was pioneered in nanosecond photodissociation studies, has been applied recently with femtosecond lasers in extensive photodissociation studies on molecules like I_2,

* Corresponding author. Fax: +31-20-444-7643.
E-mail address: mhmj@chem.vu.nl (M.H.M. Janssen).

PII: S0009-2614(01)00865-X

CH_3I, ICN [6]. So far, few femtosecond pump–probe experiments on polyatomics have been reported utilizing imaging detection techniques to map out the three-dimensional dissociation dynamics. Imaging techniques in combination with Coulomb explosion were used to study ultrafast dynamics in diatomic molecules [7,8]. Electron imaging was used to study ultrafast non-adiabatic radiationless transitions in pyrazine [9]. Very recently, Hayden et al. [10] reported the first femtosecond time resolved imaging experiment in which the three-dimensional energy and angular distribution of both the photoelectron and the photoion was obtained in coincidence. With the new coincidence technique the complete information in a femtosecond pump–probe experiment with ion and electron production can be obtained.

In this Letter we report our first femtosecond pump–probe ion imaging results using velocity map imaging to study the ultrafast photon-induced dynamics in CF_3I. This system was chosen as a prelude to investigate more complicated multi-photon induced ultrafast dynamics in small molecular systems like CF_2I_2. For the latter system various photofragment species were observed after multi-photon excitation with femtosecond pulses around 266 nm [11]. In that study TOF spectroscopic techniques were used to obtain insight on the formation mechanism, concerted versus sequential bondbreaking, of for instance the I_2 fragment formed in a multi-photon process.

The photodynamics of CF_3I after excitation with nanosecond laser pulses in the first UV absorption band has been extensively studied [12]. Excitation around 266 nm is predominantly via a parallel type transition and the major dissociation channel is CF_3 and spin–orbit excited $I^*(^2P_{1/2})$ fragments. To our knowledge no time resolved imaging experiments on CF_3I using femtosecond pulses in this UV region have been performed.

In this Letter we present femtosecond velocity map ion imaging data of the I^+ fragment. From the images we can obtain the angular and velocity distribution of the fragments. This provides information on the multi-photon absorption and subsequent femtosecond dissociation dynamics. In Section 2 we present the experimental setup, in Section 3 the measured data. In Section 4 we summarize our results and conclusions.

2. Experimental

In this section we will briefly describe our experimental apparatus. A new molecular beam machine has become operational for the study of ultrafast dynamics [13] and a more extensive description of the apparatus will be presented elsewhere [14]. The beam machine consists of three separately pumped chambers, a source chamber, a buffer chamber and the imaging chamber. In the source chamber a 1 kHz pulsed molecular beam is produced using the piezo valve pioneered by Gerlich [15]. The typical backing pressure used behind the nozzle (diameter 300 μm) is 1.1 bar. In the imaging chamber the beam is skimmed by a 2 mm hole in the repeller plate of a velocity map ion extraction lens [5]. In the center between the repeller and the extractor plates the molecular beam is crossed at right angles by the collinearly propagating femtosecond pulses. The total distance from the nozzle to the laser interaction region is 15 cm. The pulsed molecular beam is triggered by the 1 kHz clock of the regen laser amplifier system.

The commercial laser system (Spectra Physics) consists of a titanium–sapphire oscillator which produces pulses of about 80 fs duration at a repetition rate of 82 MHz. The pulses are amplified to 1 mJ in a chirped regen amplifier at 1 kHz repetition rate. A small percentage of the output of the regen is split off and monitored on line with a homebuilt single shot SHG autocorrelator equipped with a CCD detector. The typical length of the amplified pulses is about 130 fs FWHM. The amplified femtosecond pulses, which are centered around 800 nm, are doubled and tripled in BBO crystals producing pump pulses around 264 nm and probe pulses around 396 nm. The wavelength spectrum of the fundamental, the doubled and tripled pulses are monitored simultaneously by a fiberoptic coupled monochromator mounted on a PC board equipped with a linear CCD detector.

The ions produced in the laser interaction region are accelerated into a 36 cm long TOF tube. At the exit of the field free drift region the ions

impinge on a gated chevron-type micro-channel-plate. The electrons are accelerated towards a phosphor screen (P47) which is imaged by a thermo-electrically cooled slow scan CCD camera. Simultaneously, a photomultiplier detects part of the light from the phosphor screen in order to obtain the total TOF ion signal.

3. Results and discussion

In this section we report femtosecond transients and ion recoil images obtained by irradiating a cold seeded beam of CF_3I with two delayed femtosecond pulses centered at $\lambda = 264$ and 396 nm. In Fig. 1 we present an energy scheme of the known and relevant electronic states. The location of the energy levels of the various ionic parent states and dissociation channels were taken from [16,17]. As indicated in Fig. 1 an $(2 + 2')$ excitation will produce the CF_3I^+ parent ion with sufficient internal energy to enable dissociation to both $CF_3^+ + I$, and $I^+ + CF_3$ fragment channels. In Fig. 2 the pump–probe transients as measured on the CF_3I^+ parent ion mass, and the I^+ and CF_3^+ fragment masses are shown. In the TOF spectrum only these ions from the molecular beam were observed. From the literature (see also Fig. 1) it is predicted that another ionic channel, $CF_2I^+ + F$, is located at an appearance energy just below the $CF_3 + I^+(^3P_{0,1})$ channel [18]. In our TOF mass spectra we never observed any peak at the CF_2I^+ mass.

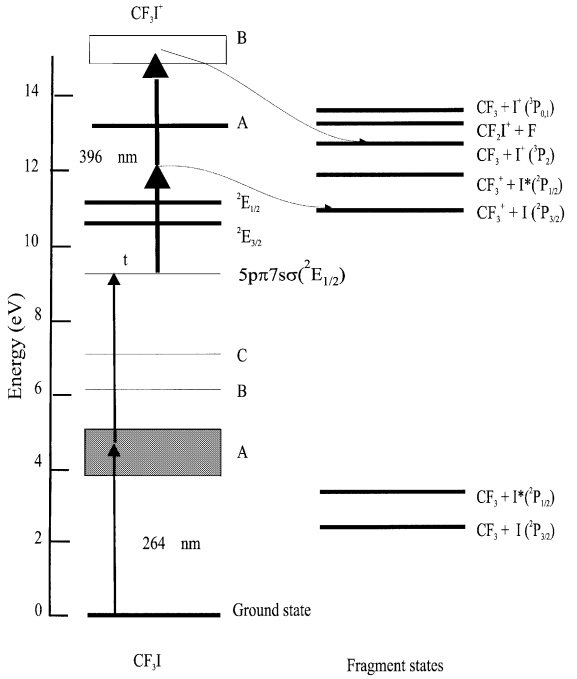

Fig. 1. Energy level diagram for the electronic states of CF_3I, CF_3I^+ and various dissociation channels. The energies of the states are taken from [16,17,23].

At short pump–probe delay a strong enhancement of all the ion peaks is observed. With the proper spatial overlap of the pulses this enhancement is 1–2 orders of magnitude larger than the sum of the ion signals from both laser pulses individually. In Fig. 2 we have normalized the intensity of each ion transient to the maximum value. The absolute magnitude of the overall ion signal of the CF_3I^+, I^+ and CF_3^+ peaks in the TOF spectrum are typically comparable within an order of magnitude. This means that both the I^+ and CF_3^+ ionic fragments are major fragment channels at the intensity levels used in our experiment. We observe for all transients an ion enhancement when the pulse at 396 nm is after the pulse at 264 nm. Therefore, we will name the pulse at 264 nm

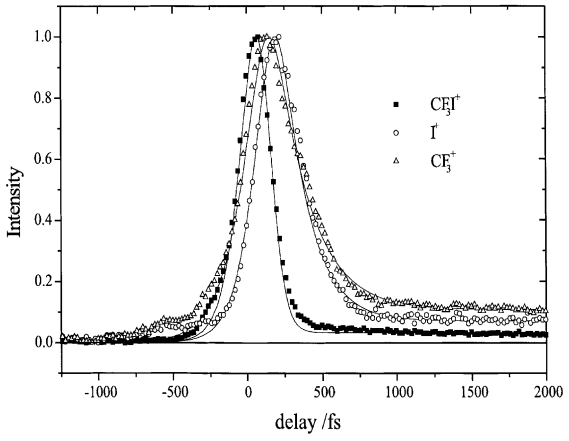

Fig. 2. Typical pump–probe transients obtained simultaneously on the different ion masses CF_3I^+, CF_3^+ and I^+, for parallel polarization of pump and probe lasers. The signal for each ion channel was normalized to the maximum value. The solid lines are the best-fit curves to the experimental transients using Eq. (1) and the constants in Table 1.

the pump pulse and the pulse at 396 nm the probe pulse, even though the energy of the pump pulse is lower. The pump laser, with a typical pulse energy of 5 μJ, and the probe laser, with a pulse energy of 20 μJ, are independently focussed with a 1000 mm and a 500 mm focal length lens, respectively. To avoid space charge effects care was taken to have both laser pulses focusing after the crossing with the molecular beam. The diameter of the pump pulse was measured with a pinhole outside the vacuum machine at the same distance from the lens as the position of the crossing of the laser with the molecular beam, and found to be about 200 μm. For our typical UV pulses with a duration of about 150 fs and energy of 5 μJ this results in an intensity of about 10^{11} W/cm^2 at the focus. This intensity is one order of magnitude lower than the typical intensity needed to align the molecules [19]. Especially for the heavy CF_3I we do not expect significant strong field alignment with this relatively short pump pulse. We estimate that around zero delay time we produce up to about 100 ions per laser shot. Care was taken to keep the laser pulse energies relatively modest. Due to the 1 kHz repetition rate of the experiment the averaged signals are built up quite rapidly.

For the transients in Fig. 2 the polarization of the probe pulse was parallel to the polarization of the pump pulse. It is found that the peak in the CF_3^+ channel is shifted by about 30 fs relative to the CF_3I^+ maximum. The peak in the I^+ channel is about 100 fs later than the parent ion maximum. At long pump–probe delay time (>1.5 ps) the intensity of the CF_3I^+ parent ion has not decayed completely to zero. There is still a small pump–probe enhancement signal, about 5% of the peak value, which appears constant on timescales of a few ps. A two-photon absorption at $\lambda = 264$ nm can potentially populate a highly excited state in CF_3I. To our knowledge there is no recent literature on the spectroscopy of highly excited states of CF_3I in the energy region around 75 760 cm^{-1}. Sutcliffe and Walsh [20], employing one-photon VUV absorption spectroscopy, observed an absorption band at 132.3 nm and tentatively assigned this to the $5p\pi^3 7s\sigma$ ($^2\Pi_{1/2}$) Rydberg state. They also observed two bands to shorter wavelengths and separated by ca. 200 and 400 cm^{-1} from the strong band at 132.3 nm. They suggested these weaker bands to be transitions to excited ν_3' vibrational levels within this Rydberg state. This means that this highly excited Rydberg state has a long enough lifetime in order to allow further excitation with the delayed probe pulse into the ionic CF_3I^+ parent state. This may explain the small constant signal detected at the CF_3I^+ parent at long pump–probe delay time. The intensity of the CF_3^+ and I^+ ionic fragments at long pump–probe delay time (>1.5 ps) was slightly dependent on the direction of the polarization of the probe beam. For perpendicular polarization the I^+ signal increased from 14% to 19%, the CF_3^+ signal increased from 17% to 22%.

The transients of the CF_3^+ and I^+ ionic fragments suggest that there are two processes contributing to the ion signals. At short pump–probe delay time there is a strong rise followed by an exponential decay. Underneath the strong peak appears a contribution from a process which has a rather long lifetime. We have fitted the fragment transients with the following expression:

$$I(t) = \int_{-\infty}^{t} [\exp(-(t' - t_0)/\tau_1) + c] \times \exp(-t'^2/2\sigma^2)\,\mathrm{d}t', \quad t' \geqslant t_0. \tag{1}$$

In Eq. (1), the first term reflects the contribution from a decaying state with a lifetime τ_1, the second part is a step-function. The second contribution, with a relative strength given by the fit parameter c, represents the long time enhancement which does not decay within our experimental accuracy on delay times of up to about 50 ps. Within our experimental time resolution we cannot distinguish a very fast exponential rise, a very slow (nanosecond) exponential decay or a simple step-function, as the proper description of the underlying mechanism for the long time decay. We decided to choose the most simple one, i.e. a step-function. The constant σ represents the time resolution of our pump–probe experiment. The best-fit parameters obtained are listed in Table 1.

A power dependence measurement of the ion signal was performed. At zero delay time the CF_3^+ signal showed a one-photon dependence on the intensity of the probe beam, and the I^+ signal a

Table 1
Parameters obtained by fitting Eq. (1) to the transients of the fragment ions

Species	t_0 (fs)	σ (fs)	τ_1 (fs)	c
CF_3I^+	0	136	50	0.01
CF_3^+	30	136	211	0.08
I^+	100	136	140	0.04

two-photon dependence on the probe beam intensity. At longer delay times the signals were too low to get sufficient statistics of the intensity dependence. Also the power dependence of the CF_3I^+ parent could not be accurately measured because of saturation of the detector. The velocity mapping ion geometry of the parent ion (which has no off-axis velocity component) focussed all the ions on a relatively small spot on the CCD detector. This resulted in a somewhat saturated signal at zero-delay time at the parent ion mass. We have not performed measurements of the power dependence of the pump laser.

Around zero delay the CF_3I^+ peak decays very rapidly. This is attributed to a $(1+2')$ process, where the wavepacket rapidly moves on the dissociative A-band surface away from a favorable geometry and energy for ionization to the ground state of the ionic parent. The CF_3^+ and I^+ transients around zero delay have a somewhat shifted peak position and slower decay. We think this is due to a $(2+1')$ process for CF_3^+ and a combination of $(2+2', 1+3')$ processes for the I^+ channel. The short delay of $t_0 = 30$–100 fs may be caused by fast dynamics in the excited $5p\pi 7s\sigma$ ($^2E_{1/2}$)-Rydberg state needed to provide a favorable geometric change for dissociative ionization. However, this dynamics may subsequently also lead to spread of the excited wavepacket into a configuration which has much lower dissociative ionization efficiency resulting in the decay of the ionic signal to the constant small long time enhancement. See also the following discussion of the ion images.

We will now turn to the presentation and discussion of the angular resolved scattering data using the imaging detector. We have measured at fixed pump–probe delay times the angular and velocity distributions of the I^+ and CF_3^+ fragments. In the parallel pump–probe configuration I^+ images were recorded at 100 fs interval, for CF_3^+ at 200 fs interval. Fig. 3 shows velocity map images

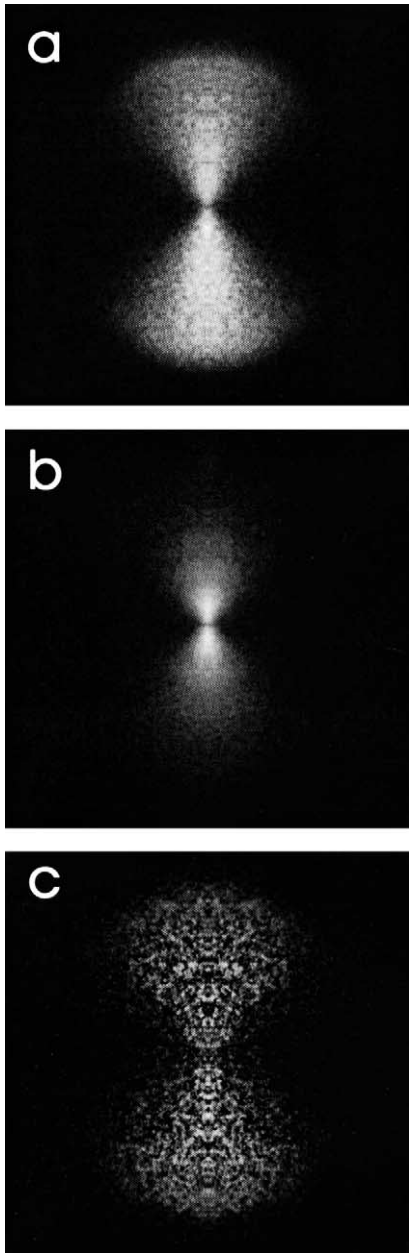

Fig. 3. Velocity map images of the I^+ fragment at (a) 0 fs (b) 200 fs and (c) 1000 fs pump–probe delay. All images are taken with a parallel polarization of pump and probe laser, which is vertical and in the plane of the images.

of I^+ at delay times of 0, 200 and 1000 fs. All the images shown are the result of subtracting the background images produced by each of the pump and probe lasers separately. A typical single image was recorded in a few minutes. Because of the high repetition rate of the 1 kHz laser system, accumulation of signal on the CCD chip is a factor of 100 faster than in the low repetition rate photodissociation experiments on oriented CH_3I using nanosecond pulsed lasers and the same imaging camera [21].

At zero delay time (panel (a) in Fig. 3) the image (size 450×450 pixels) appears quite anisotropic with fragments recoiling predominantly along the vertical direction of the polarization of the pump and probe pulses. At slightly longer delay time, 200 fs (panel (b) in Fig. 3), the intensity distribution of I^+ fragments in the image is concentrated at much smaller distances from the center of the image. This indicates that at this delay time, the recoiling I^+ fragments are produced with much lower kinetic energy. At long time delay, 1000 fs (panel (c) in Fig. 3), the fragments recoil with larger velocities again.

Because the polarization of the pump and probe pulses are parallel and in the plane of the CCD detector we can use the inverse Abel-transform to obtain the three-dimensional distribution. From the inverted image the kinetic energy distribution of the photofragments was obtained by integration over all recoil angles. The results are shown in Fig. 4. As can be seen the kinetic energy distribution changes dramatically when increasing the time delay from 0 to 200 fs. At long time delay the recoil energy is again quite similar to the distribution at zero time delay.

Insight into the dynamics responsible for these kinetic energy distributions can be obtained from an inspection of the energetics for various pump–probe processes. The threshold energy for production of the lowest $I^+(^3P_2) + CF_3$ channel is 12.7 eV (see Fig. 1). This means that an excitation involving two pump photons at 264 and one probe photon at 396 nm is not enough (12.5 eV) to access this lowest $I^+(^3P_2) + CF_3$ channel. However, two photons each of the pump and probe pulses amount to 15.6 eV and provide enough energy for the CF_3I molecule to access all I^+ dissociation

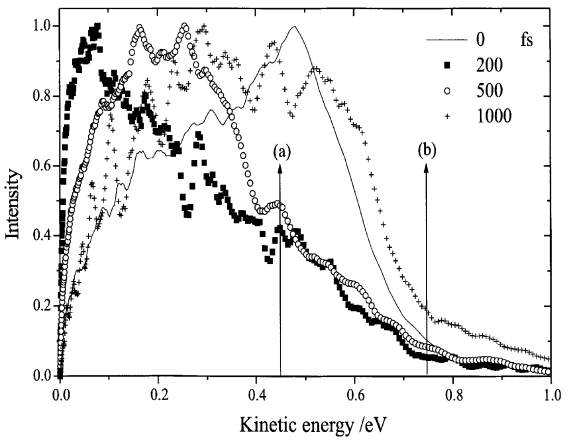

Fig. 4. Kinetic energy release of the I^+ fragment as derived from the Abel-inverted three-dimensional images. The arrows indicate the energetic cut-off for a $(2+2')$ photoexcitation, assuming an electron energy of 0.85 eV for $I^+(^3P_{0,1})$ (a) and $I^+(^3P_2)$ (b) fragments (see text).

channels. A $(2+2')$ excitation is in agreement with the measured squared dependence of the I^+ signal on the intensity of probe laser. As is seen in Fig. 4, a bimodal structure is observed at zero delay and 1000 fs delay. There appears to be a low kinetic energy region from 0 to 0.45 eV and a high energy region from 0.45 to 0.74 eV. In Fig. 4 these two regions are marked by arrows. The position of these arrows indicate the energetic cut-off of the available energy for the photofragments assuming an energy of the ejected electron of 0.85 eV. Unpublished results from very recent photoelectron-photoion coincidence experiments [22] show a strong peak in the photoelectron spectrum at an energy of 0.85 eV. If the dissociation dynamics is resulting from a $(2+2')$ photon absorption we can calculate that for the lower channel $I^+(^3P_2) + CF_3$ we have a maximum of 0.74 eV kinetic energy available for the $I^+(^3P_2)$ fragment. For the higher channel $I^+(^3P_{0,1}) + CF_3$ this results in a maximum of 0.44 eV kinetic energy for the $I^+(^3P_{0,1})$ fragment. These energetic cut-off values are in very good agreement with the experimentally observed bimodal kinetic energy distribution of the I^+ fragment, see Fig. 4.

At short time delays around 200 fs we observe a much smaller kinetic energy release of the I^+ fragment. It appears that at these times, close to

the maximum of the I^+ transient (see Fig. 2), another process may be responsible for the production of the I^+ fragment. If we assume the fragmentation results from a $(1+3')$ photon process we excite the CF_3I molecule with 14.08 eV of energy. If again an electron with a kinetic energy of about 0.85 eV is ejected, we can only reach the lower $I^+(^3P_2)+CF_3$ channel. It allows the $I^+(^3P_2)$ fragment to leave with at most 0.19 eV. The higher $I^+(^3P_{0,1})+CF_3$ channel can only be reached when electrons with energies less than 0.52 eV are ejected, leaving very little energy available for recoil energy. This means that from an energetic point of view the process is likely to result from a $(1+3')$ photon absorption. The one-photon absorption at 264 nm excites into the A-band and induces dissociation of CF_3I. During the dissociation the extending molecule may pass a region where there is good Frank–Condon overlap with the dissociative excited $\tilde{A}$ state in the CF_3I^+ parent ion. A three-photon excitation with the 396 nm probe laser, possibly enhanced by quasi-resonances with highly excited states in the neutral molecule, can promote the system to an ionic curve resulting in low kinetic energy release. At longer timescales the molecule has fully dissociated and this pathway will not be accessible anymore. A $(1+3')$ multi-photon pathway may explain the dramatic change in the kinetic energy release of the I^+ fragment.

Besides the energy distribution of the recoiling ionic fragments also the angular recoil distribution can be obtained from the Abel-inverted images. For the two I^+ channels the angular distribution was extracted by integrating the I^+ ion yield within different energy regions. In Fig. 5 the angular distribution at zero delay time is shown for I^+ ions with kinetic energy between 0.45 and 0.8 eV. The angular distributions were fitted to the following expression:

$$I(\theta_s)=\frac{\sigma}{4\pi}[1+\beta P_2(\cos\theta_s)+\gamma P_4(\cos\theta_s)+\cdots], \tag{2}$$

where θ_s is the laboratory polar angle between the direction of the recoil velocity and the vertical direction of the polarization of the laser pulses. The functions $P_2(\cos\theta_s)$, $P_4(\cos\theta_s)$ are Legendre polynomials. The best-fit coefficients β and γ, extracted for the three kinetic energy regions as a function of delay time, are shown in Table 2. From the fit we find that for the high kinetic energy channel correlating with the $I^+(^3P_2)$ fragment channel, the extracted $\beta=3.0$ and $\gamma=1.9$. These values are quite high indicating that the fragments are ejected with a very anisotropic angular distribution. We can compare these values with what would be expected for a purely parallel multi-photon transition. For a two-photon transition and fast axial recoil the angular distribution $I(\theta_s)\propto\cos^4\theta_s$. When we expand this $I(\theta_s)$ in Legendre polynomials, as in Eq. (2), we obtain $\beta=2.86$ and $\gamma=1.14$. For a pure four-photon parallel transition $I(\theta_s)\propto\cos^8\theta_s$, we find $\beta=3.64$ and $\gamma=3.0$. The slightly lower β and γ parameters at zero delay time for the fast $I^+(^3P_2)$ fragment channel than those expected for a pure parallel fast axial four-photon transition may be caused by several reasons. First of all the transition may be effected by non-parallel transitions. In fact, the

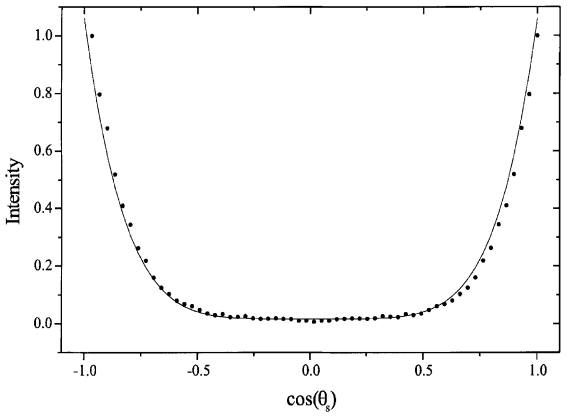

Fig. 5. Angular distribution of I^+ fragments at 0 fs delay and with kinetic energy in the 0.45–0.8 eV region.

Table 2
Legendre expansion of the angular distributions of the I^+ fragment integrated in three different energy regions

E_{kin} (eV)	0–0.1	0.1–0.45	0.45–0.8
τ (fs)	β,γ	β,γ	β,γ
0	2.0 0.8	2.9 1.6	3.0 1.9
200	1.8 0.8	2.7 1.4	2.0 1.6
500	1.6 0.6	2.7 1.4	2.4 1.6
1000	1.8 0.9	2.5 1.5	2.1 1.4

two-photon pump excitation is resonant at the one-photon level with the A band. According to Kavita and Das [12] the one-photon absorption at 266 nm in the A-band of CF_3I is composed of an excitation to two surfaces, which is 90% parallel and 10% perpendicular in nature. Furthermore, the two-photon probe step exciting the CF_3I^+ parent in the region just above the $\tilde{B}$ state may have a mixed character. A second cause for the reduction of the anisotropy of the angular recoil distribution of the I^+ fragment is dynamics in the excited ionic state. A finite lifetime of the ionic state may result in a rotation of the symmetry axis of the molecule before fragmentation. This reduces the observed anisotropy [24]. The $\tilde{B}$ state is adiabatically coupled with the fast $I^+(^3P_2)$ exit channel, but does not adiabatically couple with the $I^+(^3P_{0,1})$ states [17]. The lower anisotropy observed in the$I(^3P_{0,1})$ channel (see Table 2) is possibly due to a longer dissociation time for fragmentation into the $I^+(^3P_{0,1}) + CF_3$ channel. Downie and Powis [17] have observed a similar effect for dissociation at ionic excitation energies around 13.5 eV. They observed energy dependent lifetimes of 0.2–4.0 ps with a faster decay with increasing ionization energy. To obtain more quantitative information on these effects we are currently studying the polarization dependence of the ion images. Furthermore, the images obtained for the CF_3^+ fragment will also help in understanding the effect and polarization dependence of the intermediate $5p\pi^3 7s\sigma$ $(^2\Pi_{1/2})$ Rydberg state. These results will be published elsewhere [14].

4. Conclusions

Ultrafast photodynamics in CF_3I were studied with the femtosecond pump–probe technique and velocity map ion imaging. The velocity and angular distributions of I^+ fragments were recorded as a function of delay time between pump, 396 nm, and probe, 264 nm. The velocity distribution of I^+ photofragments shows a dependence on the delay time. The energy distribution can be correlated to the two major I^+ fragment channels. The anisotropy of the recoil distribution is strong and dominated by the order of the multi-photon process for fast I^+ fragments. This indicates rapid, axial recoil dynamics of the excited ionic states accessed at these energies and dissociating in fast $I^+(^3P_2)$ photofragments. Velocity map ion imaging of femtosecond photodynamics in CF_3I is shown to be a powerful technique to elucidate the multi-photon induced fragmentation dynamics of highly excited states in polyatomic molecules.

Acknowledgements

The research has been financially supported by the councils for Chemical Sciences and Physical Sciences of the Netherlands Organization for Scientific Research (CW-NWO, FOM-NWO). W.R. gratefully acknowledges CW-NWO for a PhD fellowship within the Young Chemists Program. The authors would like to thank Prof. S. Stolte for his support and Dr. D.W. Chandler for his initial help in the imaging experiments. Mr. W. Feijen is acknowledged for his help in implementing various software programs for analysis of the imaging data.

References

[1] D.W. Chandler, P.L. Houston, J. Chem. Phys. 87 (1987) 1445.
[2] D.W. Chandler, D.H. Parker, Adv. Photochem. 25 (1999) 56.
[3] A.H. Zewail, J. Phys. Chem. A 104 (2000) 5660.
[4] M.H.M. Janssen, M. Dantus, H. Guo, A.H. Zewail, Chem. Phys. Lett. 214 (1993) 281.
[5] A.T.J.B. Eppink, D.H. Parker, Rev. Sci. Instrum. 68 (1997) 3477.
[6] D.P. Zhong, A.H. Zewail, J. Phys. Chem. A 102 (1998) 4031.
[7] J.J. Larsen, N.J. Morkbak, L. Olesen, N. Bjerre, M. Machholm, S.R. Keiding, H. Stapelfeldt, J. Chem. Phys. 109 (1998) 8857.
[8] S. Chelkowski, P.B. Corkum, A.D. Bandruk, Phys. Rev. Lett. 82 (1999) 3416.
[9] T. Suzuki, L. Wang, H. Kohguchi, J. Chem. Phys. 111 (1999) 4859.
[10] J.A. Davies, J.E. LeClaire, R.E. Continetti, C.C. Hayden, J. Chem. Phys. 111 (1999) 1.
[11] W. Radloff, P. Farmanara, V. Stert, E. Schreiber, J.R. Huber, Chem. Phys. Lett. 291 (1998) 173.

[12] K. Kavita, P.K. Das, J. Chem. Phys. 112 (2000) 8426, and references therein.
[13] W. Roeterdink, A.M. Rijs, G. Bazalgette, P. Wasylczyk, A. Wiskerke, S. Stolte, M. Drabbels, M.H.M. Janssen, in: R. Campargue (Ed.), Atomic and Molecular Beams, Springer, Berlin, 2000, p. 405.
[14] W. Roeterdink, M.H.M. Janssen, to be submitted.
[15] D. Gerlich, private communication.
[16] L.D. Waits, R.J. Horwitz, R.G. Daniel, J.A. Guest, J.R. Appling, J. Chem. Phys. 97 (1992) 7263.
[17] P. Downie, I. Powis, Faraday Discuss. 115 (2000) 103.
[18] I. Powis, O. Dutuit, M. Richard-Viard, P.M. Guyon, J. Chem. Phys. 92 (1990) 1643.
[19] S.T. Althorpe, T. Seideman, J. Chem. Phys. 110 (1999) 147.
[20] L.H. Sutcliffe, A.D. Walsh, Trans. Faraday Soc. 57 (1961) 873.
[21] M.H.M. Janssen, J.W.G. Mastenbroek, S. Stolte, J. Phys. Chem. A 101 (1997) 7605.
[22] A.M. Rijs, C.C. Hayden, M.H.M. Janssen, work in progress.
[23] M.E. Jacox, J. Phys. Chem. Ref. Data 17 (1988) 455.
[24] S. Yang, R. Bersohn, J. Chem. Phys. 61 (1974) 4400.